

Calculation of the electromagnetic field in a multimode microwave cavity for sintering planar-perovskite SOFC ceramics

K. Darcovich · J. Biton · J. Magnier

Received: 26 September 2005 / Accepted: 17 July 2007 / Published online: 13 August 2007
© Springer Science + Business Media, LLC 2007

Abstract In the context of developing a full scope numerical simulation of microwave sintering, a more precise and fundamentally based method of calculating the electromagnetic field strengths was sought. The finite difference time domain (FDTD) method was adopted and implemented for this purpose. The temporal nature of the electromagnetic fields was studied to ensure stable algorithms for determining root mean square values for field strengths. Further, a method was outlined whereby the multimode nature of a cavity can be determined with quality parameters for the source frequency. A example calculation is given for lanthanum nickelate, a potential solid oxide fuel cell cathode material with a complex microwave response, arising from its significant dielectric and magnetic loss properties.

Keywords FDTD method · Electromagnetic fields · Multimode cavity · SOFC materials

NRCC No. 49120.

K. Darcovich (✉)
National Research Council of Canada, Institute for
Chemical Process and Environmental Technology,
Ottawa, Ontario K1A 0R6, Canada
e-mail: ken.darcovich@nrc-cnrc.gc.ca

J. Biton
ICAM-Nantes, 35, av. du Champ des Manoeuvres,
Carquefou 44470, France

J. Magnier
École Nationale Supérieure de Céramique Industrielle,
47-73, av. Albert Thomas, 87065 Limoges Cedex, France

1 Introduction

A solid oxide fuel cell (SOFC) is an electrochemical device that converts the energy of a chemical reaction directly into electrical energy. With a solid electrolyte and high operating temperature, it offers many advantages over conventional power-generating systems in terms of efficiency, reliability, modularity, fuel flexibility, and environmental friendliness.

Potentially interesting classes of materials for SOFC cathodes are good candidates for processing by microwave sintering. Some K_2NiF_4 -type structures which have higher thermal stability, exhibit significant dielectric and magnetic responses to microwave energy, making them highly suitable for this type of processing. It is argued that electromagnetic fields can reduce the sintering activation energy, allowing morphology changes at lower temperatures than could be achieved conventionally [1, 2]. At SOFC service temperatures of around 800°C, some of these K_2NiF_4 -type microstructures have infinitesimal ionic diffusion rates, and are thus thermally stable with respect to this principle mechanism of SOFC material degradation. The material considered in the present study, La_2NiO_4 , was shown to belong to the K_2NiF_4 -type class of materials [3].

The penetration of microwaves into materials gives rise to a volumetrically distributed heat source. The process combines the propagation and absorption of electromagnetic waves in the ceramic material and heat transport within the body, inducing changes to both macroscopic shape and microstructural morphology [4].

Energy transfer in microwave-matter interactions can be described by the generalized energy loss equation [5]:

$$P_{\text{MW}} = 2\pi [\epsilon_0 \epsilon'_R \tan \delta |E|^2 + \mu_0 \mu'_R \tan \phi |H|^2] \quad (1)$$

where ϵ_0 and μ_0 are dielectric permittivity and magnetic permeability of free space, ϵ'_R and μ'_R are the real part of the dielectric permittivity and magnetic permeability of the sample processed, $\tan \delta$ and $\tan \phi$ are the dielectric and magnetic loss factor values, and $|E|$ and $|H|$ are the electric and magnetic field strength inside the sample. Although both E and H fields appear above, most research to date has not considered the magnetic contribution. Dielectric and magnetic loss can lead to uneven heating and thermal runaway in materials with improper microstructural design and/or low thermal conductivity.

The microwave heating of La_2NiO_4 solid oxide fuel cell material has been demonstrated to have a significant magnetic contribution [6]. This feature is important, since a greater amount of energy for sintering is extracted from the standard microwave input. This property enables a more precise application of energy for sintering for cases such as La_2NiO_4 , without the need for extremely high temperatures, thereby facilitating processing which tailors the material microstructure for SOFC requirements.

To obtain the temperature distribution by numerical simulation in the sample at each time step, the heat transport equation must be solved with the appropriate boundary conditions. It incorporates the conversion of microwave energy to thermal energy, as well as thermal losses to the environment. For the 2D case, this equation is:

$$\frac{\rho c}{k_T} \frac{\partial T}{\partial t} = \frac{\partial^2 T}{\partial x^2} + \frac{\partial^2 T}{\partial y^2} + P_{\text{MW}}(x, y, t) - Q_R - Q_C \quad (2)$$

where c is the heat capacity per unit volume, ρ the density, T the temperature, t the time, k the thermal conductivity, P_{MW} the microwave power, Q_R the radiation heat transfer and Q_C the convection heat transfer.

To proceed with spatially resolved sintering simulations, accurate field values of E and H are required in Eq. 1. Here is the point of departure for the present work, where an improved formulation is developed to determine and input electric and magnetic field strengths. Previously, empirical models were used, where for example, the electric field is assumed to decay (at a position x) within the sample according to:

$$E = E_0 \exp\left(\frac{-x}{d}\right) \quad (3)$$

where d is the skin depth and E_0 is the electric field in the unloaded cavity, which is proportional to the microwave power temporal profile [7].

Models such as Eq. 3 are based on simplifications of the solutions of Maxwell's equations which govern electromagnetic fields. It is thus the purpose of this project to apply solutions of Maxwell's equations over geometry corresponding to the cavity found in a microwave oven, powered by a magnetron in multimode operation.

2 Theoretical basis

Electromagnetic fields are interdependent and propagate according to the equations outlined by Maxwell.

The electric (\vec{E}) and magnetic (\vec{H}) fields are given by,

$$\nabla \times \vec{H} = \frac{\partial \vec{D}}{\partial t} + \vec{J} \quad (4)$$

$$\nabla \times \vec{E} = -\frac{\partial \vec{B}}{\partial t} \quad (5)$$

$$\nabla \cdot \vec{D} = \rho_e \quad (6)$$

$$\nabla \cdot \vec{B} = 0 \quad (7)$$

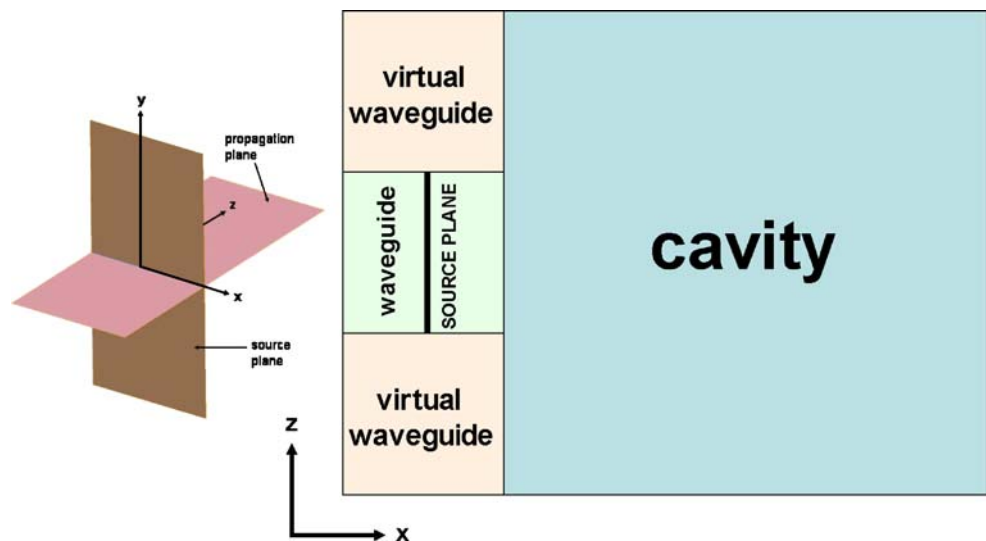
Above, $\vec{D} = \epsilon \vec{E}$ and $\vec{B} = \mu \vec{H}$, for materials which are non dispersive and isotropic, with ϵ being the dielectric constant and μ is the magnetic permeability. The parameter ρ_e is the current density, and \vec{J} is the current related to Ohm's law by $\vec{J} = \pm \sigma_e \vec{E}$ where σ_e is the electrical conductivity of the material.

3 Numerical implementation

The discretization employed in this project was based on the method of Yee [8] which expressed Maxwell's curl equations in their finite-difference form. This is a commonly implemented form for electrodynamic simulations known as the finite-difference time domain (FDTD) method, details of which can be found in [9].

The FDTD method was developed and refined extensively during the 1990s. Many of the numerical features employed here come from the volume of work demonstrating advances on Yee's original concept [8] to treat multimode systems [10], as well as three dimensional systems [11]. The present model contributes advances in both these areas. Where previously, microwave systems were demonstrated with assumed modes assigned equal amplitudes, the present study employs a frequency distribution to determine

Fig. 1 Reference planes for input plane waves and propagation plane. On the right, the finite difference domain is shown, indicating the cavity, waveguide, source plane and virtual waveguide sections



the resonant modes of non-uniform amplitude, corresponding to the real system parameters, energy level and waveguide and cavity geometry [12]. Previous multimode treatments also involved a curve fitting method of mode contributions to match experimentally determined field strengths patterned on liquid crystal sheets [13]. The present method for determining these modes for the FDTD method is detailed in Sections 5.1.2 and 6 of this paper. For cases where the mode index m was even, the FDTD method had to be adapted by implementing virtual waveguides (Section 6.1) of extended (numerical) dimension. The implementation of virtual waveguides to permit inclusion of some resonant modes in the cavity represents a novel contribution to the FDTD method of simulation microwave fields. Previous work was also limited by computational

resources [14]. Multi-grid methods and empirical approaches to multimode behaviour was required to achieve reasonable resolution for loaded cavities [14]. The present work is able to treat a multimode system, considering all resonating TE and TM modes, with both dielectric and magnetic contributions, in three dimensions.

Multiple modes of electromagnetic propagation will occur in a microwave system as a result of resonance arising in the cavity for frequencies whose wavelengths are in close proportion to the physical dimension of the cavity into which they are emitted. Modes are described with labels TE and TM to denote respectively transverse electric and transverse magnetic propagation. These modes are further subscripted as TE_{mnl} , where m, n and l are integers (including zero) representing the

Fig. 2 Calculated electric field in microwave cavity with TE_{11} source in waveguide

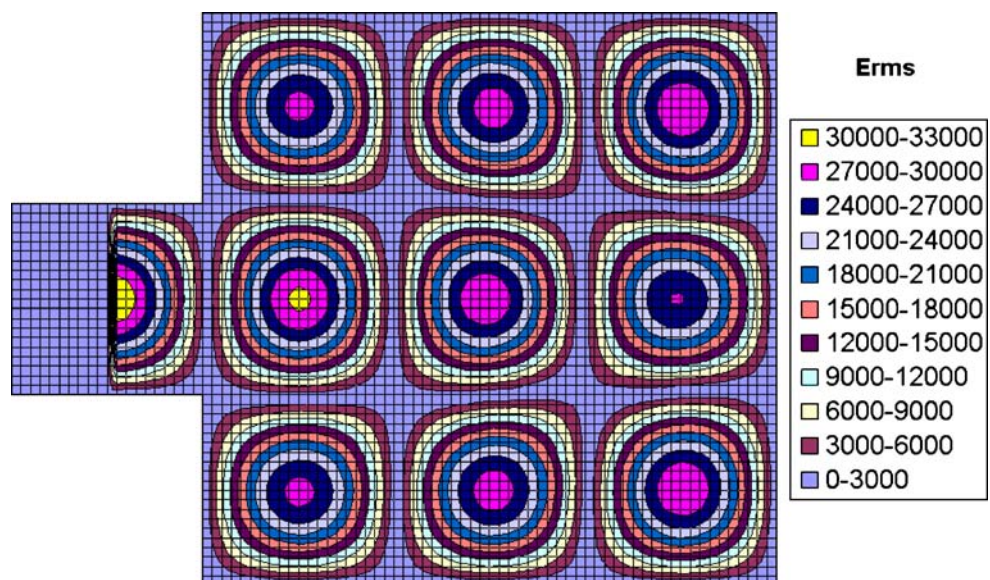
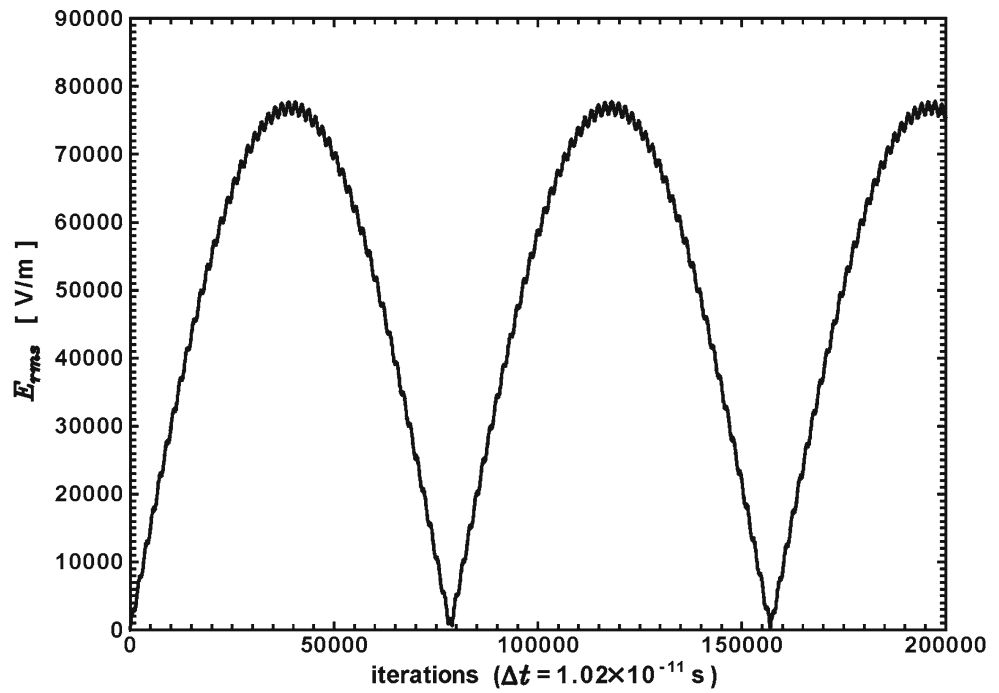


Fig. 3 Point values of the absolute values of E_z calculated over many iterations in an empty cavity. Calculated at node (30,30), an E_z extremum



number of half-wavelengths in the x , y and z directions in the cavity under consideration [15]. In a two dimensional simulation, only two indices are needed.

3.1 Microwave source

For TE modes, microwave energy input into cavities propagating in the z -direction, is represented as plane waves given by the real components of:

$$\begin{aligned}
 E_x &= \frac{j\omega\mu H_0 n\pi}{k_c^2 d} \cos \frac{m\pi x}{a} \sin \frac{n\pi z}{d} \exp j(\omega t - \beta y) \\
 E_y &= 0 \\
 E_z &= -\frac{j\omega\mu H_0 m\pi}{k_c^2 a} \sin \frac{m\pi x}{a} \cos \frac{n\pi z}{d} \exp j(\omega t - \beta y) \\
 H_x &= -\frac{j\beta H_0 m\pi}{k_c^2 a} \sin \frac{m\pi x}{a} \cos \frac{n\pi z}{d} \exp j(\omega t - \beta y) \\
 H_y &= -H_0 \cos \frac{m\pi x}{a} \cos \frac{n\pi z}{d} \exp j(\omega t - \beta y) \\
 H_z &= -\frac{j\beta H_0 n\pi}{k_c^2 d} \cos \frac{m\pi x}{a} \sin \frac{n\pi z}{d} \exp j(\omega t - \beta y) \quad (8)
 \end{aligned}$$

The relation between the magnetic and electric field strengths is given by,

$$H_0 = \left(\frac{\epsilon}{\mu} \right)^{\frac{1}{2}} E_0 \quad (9)$$

Fig. 1 shows a schematic representation of the geometry and orientation used in this project.

3.2 Wall treatment

The cavity walls are made of conducting metal. In such cases, the wall conditions for the electric and magnetic fields are given by,

$$\vec{n} \times \vec{E} = 0 \quad (10)$$

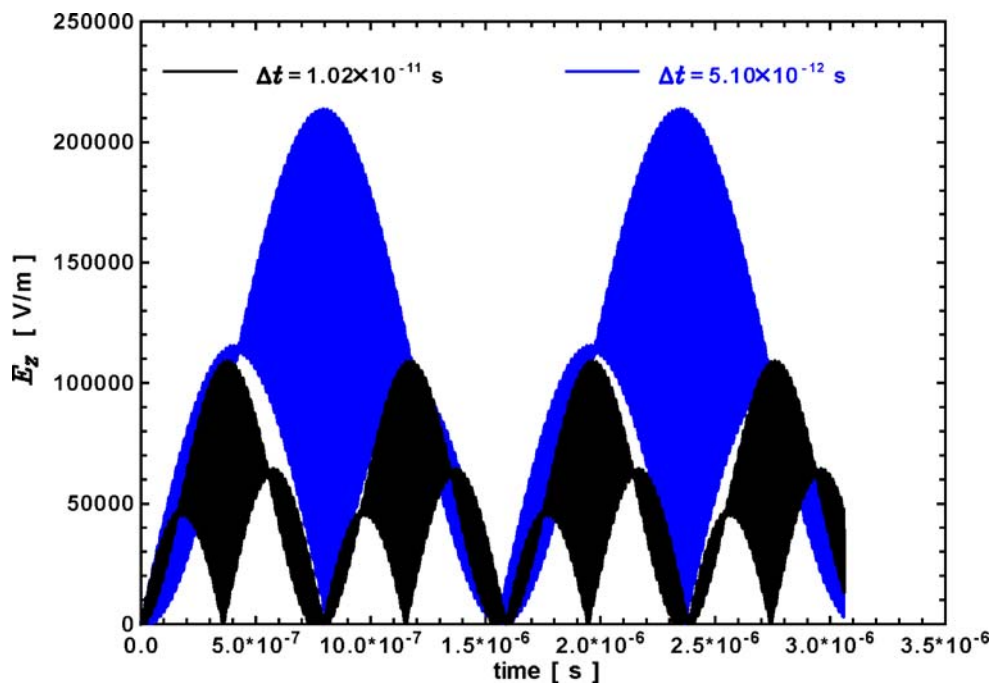
$$\vec{n} \cdot \vec{H} = 0 \quad (11)$$

More simply, the tangential components of the electric field, and the normal components of the magnetic field are zero.

3.3 System parameters

A microwave source operating at 2.45 GHz was modelled in this work. Because of the high frequency, very short time steps were necessary to maintain numerical stability. A time step of 10^{-11} s was determined, based on the Courant stability criteria [16]. Electromagnetic field strengths calculated on this short time scale must be integrated over a sufficient period of steps as it will be shown later in this paper that the field is temporal in nature.

Fig. 4 Point values of the absolute values of E_z calculated over many iterations in an empty cavity as a function of time step. The calculation period for E_{RMS} values is shown to be dependent on Δt , but the values of E_{RMS} remain constant. Calculated at node (30,30), an E_z extremum

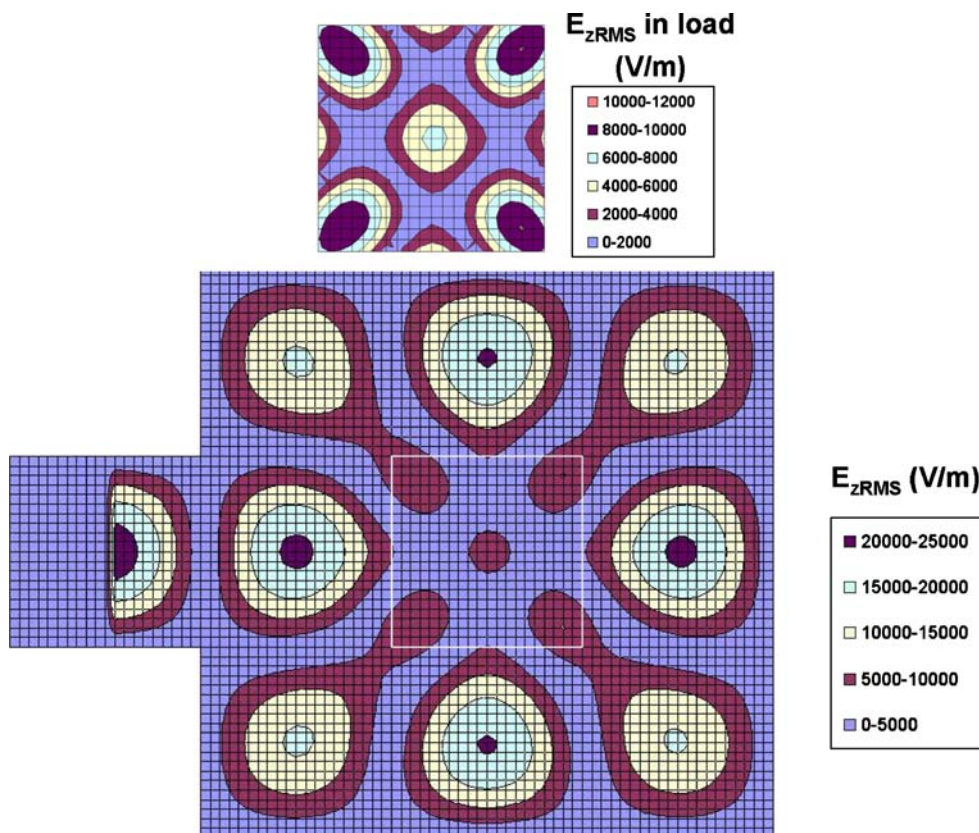


4 Code validation

A two-dimensional result published by Clemens and Saltiel [17] was used to validate the code which was

written for this project. For this test, a 60×60 grid was used with a 20×20 section for a waveguide. The grid spacings were determined by $\sqrt{2}\gamma_0/40 \cong 4.329$ mm, and the time step $\Delta t = \Delta x/\sqrt{2}c_0 \cong 1.02 \times 10^{-11}$ s.

Fig. 5 Calculated field of E_z with a load centered in the cavity. The inset details the electric field inside the load



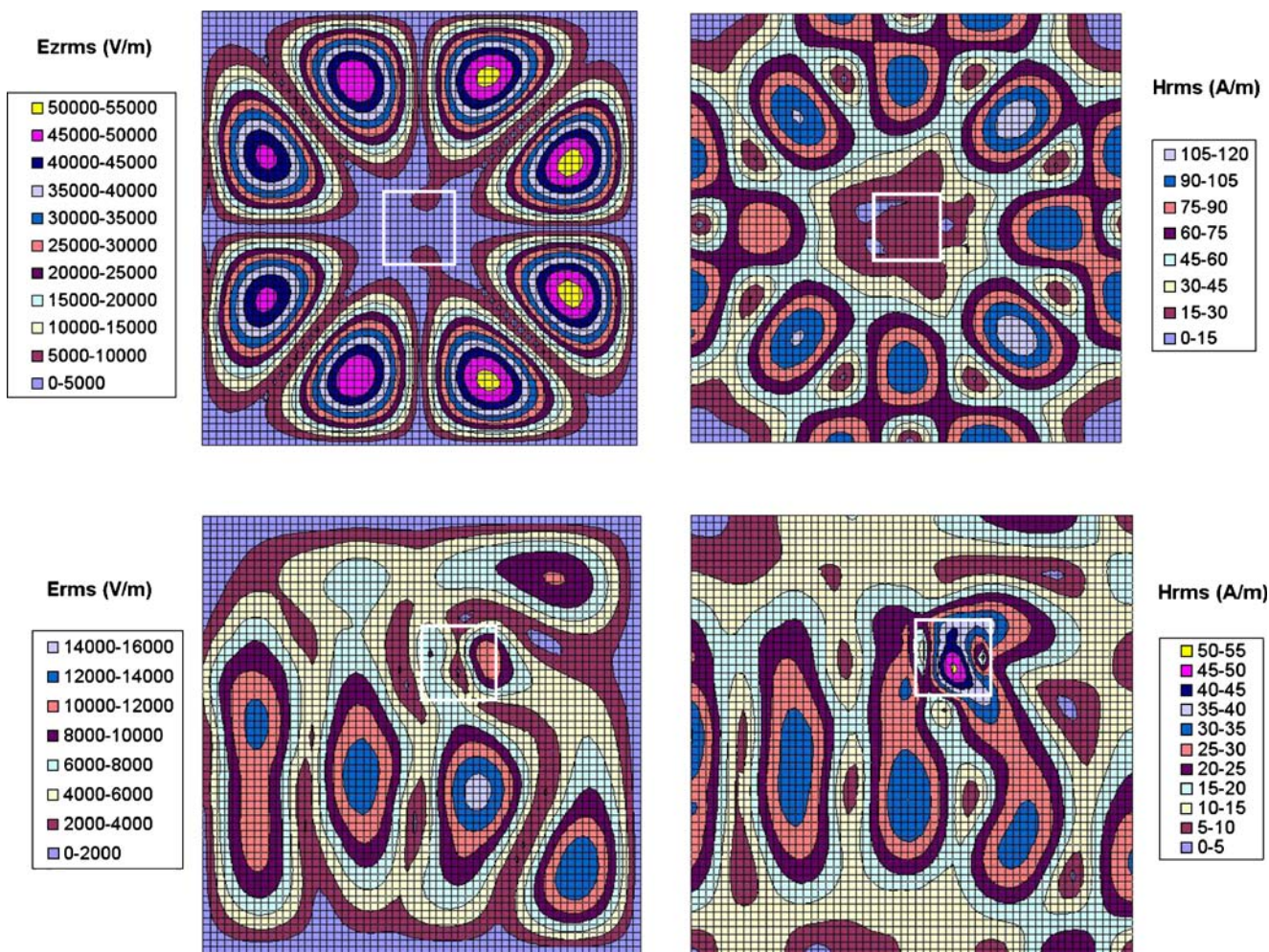


Fig. 6 Calculated E and H fields for loaded cavities. The top images show a small load in the center, the lower ones show an off-center load

The mode TE_{33} was modelled in an empty cavity, thus the mode TE_{11} in the waveguide. The value of E_0 was set as 1000 V/m, the value $\varepsilon_{r,\text{air}}$ was 1.006, $\mu_{r,\text{air}}$ was 1 and the electrical conductivity of air, $\sigma_{\text{air}} = 2 \times 10^{-10}$.

The code was allowed to run for 10 000 time steps, at which point a root mean square (RMS) average of the electric field was calculated over 20 iterations. Figure 2 shows a contour plot of the results, which qualitatively and quantitatively match the results given in Fig. 2(a) of Clemens and Saltiel [17]. Perturbing the source frequencies to values 10% above and below 2.45 GHz produced non-resonant patterns which also matched the results of Clemens and Saltiel.

5 Temporal analysis of the fields

For empty and loaded cavities, distinctly different temporal behaviour of the electromagnetic fields was

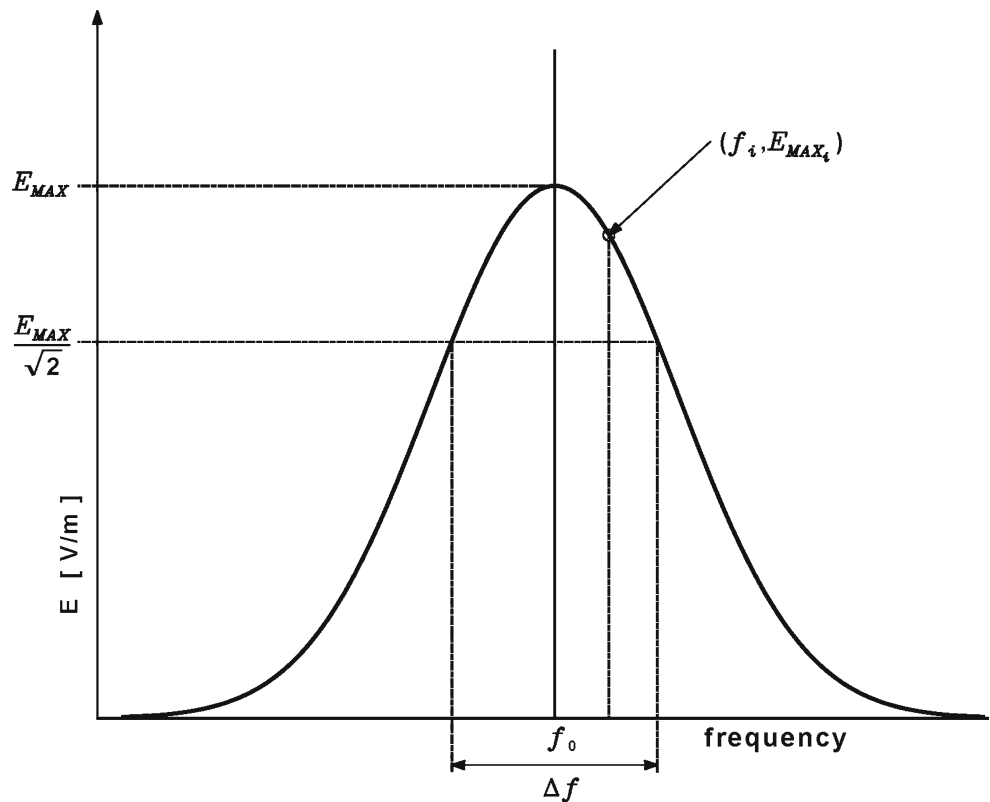
observed. The temporal variation was therefore treated according to the load state of the cavity.

5.1 Empty cavity

5.1.1 Time steps

Figure 3 shows the calculated electric field strength E_{RMS} for a node in an empty cavity, traced over many iterations. The variation is periodic, and also shows a sub-level of oscillation over its major period. The behaviour shown in Fig. 3 is typical of resonant electromagnetic fields. Thus, in order to determine a root mean square (RMS) value of the field strength (ie; $E_{\text{RMS}} = \sqrt{\frac{\sum_{i=1}^n E_i^2}{n}}$), the summation period must be correctly chosen to coincide with the periodic behaviour of the fields. For the case shown, 75,720 iterations comprise one period, a real time duration of 7.8×10^{-7} s. The E_{RMS} value determined in this way

Fig. 7 Schematic of the frequency spectra centered on the unit specification, f_0 . The quality factor Q , determines Δf , and off center resonant frequencies f_i will have a source amplitude E_{MAX_i}



is suitable for microwave heating since a suitable time scale there is 0.1 s.

There appears to be a numerical effect at work since the functionality of E_z depends on the time step chosen. If the time step used in the previous example is cut in half, the number of iterations required to complete a full period is quadrupled. In this case, the identical value of $E_{RMS} = 55109$ V/m is obtained, which requires a longer calculation period of 15.6×10^{-7} s. Figure 4 shows the absolute values of E_z taken at the same nodes as the E_{RMS} values in Fig. 3. Figure 4 shows results for the two time steps mentioned above, 1.02×10^{-11} s, and 5.1×10^{-12} s. In terms of the computational algorithm adopted, tracing E_{RMS} values identifies the peak of the periodic resonance. Knowing that a symmetrical temporal form exists, efficiency is gained by calculating E_{RMS} over only a half period.

5.1.2 Cavity dimensions

The results calculated for code validation can be shown to be highly sensitive to small perturbations in the cavity dimensions. In order to reproduce the results of Clemens and Saltiel [17], dimensions which were exact multiples of wavelengths were required. Changes of

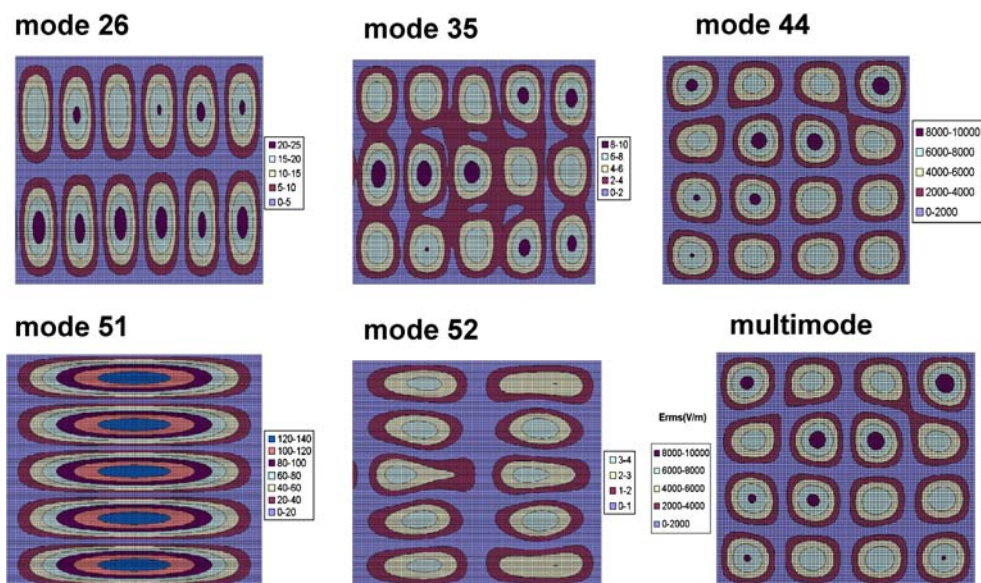
plus or minus 0.5 and 1.0% respectively in the cavity dimension produced E_{RMS} average values of only 10.3 and 5.9% of the peak electric field strengths in a cavity perfectly dimensioned for TE₃₃ resonance. These results underline the importance of using highly precise calculations.

Connected to the issue of cavity dimensions are the multimode qualities of the system. Cavity dimensions are key parameters in determining which modes can propagate inside it. Resonant conditions can be achieved for modes of indices mnl when the following condition is satisfied [18] in a rectangular cavity of dimension abd :

$$\left(\frac{2}{\gamma_i}\right)^2 = \left(\frac{m}{a}\right)^2 + \left(\frac{n}{b}\right)^2 + \left(\frac{l}{d}\right)^2 \tag{12}$$

Real microwave sources emit in a range of frequencies centered on a main frequency which is usually cited in the specifications of the device, 2.45 GHz in this case. As such, there can be multiple solutions to Eq. 12, where different values of γ_i from within the emitted range of frequencies correspond to distinct trios of mnl , each producing a mode, which when taken together, result in a multimode microwave cavity.

Fig. 8 The TE fields for the five modes determined in Table 1, as well as the overall field which is a summation of the five contributing modes



5.2 Loaded cavity

The temporal behaviour of a loaded microwave cavity differs from that of an empty one. For a loaded case, the E_{RMS} values increase steadily over a short number of iterations (ie; well under 5000), and then stabilize. A simple check in the algorithm that the E_{RMS} are no longer varying over time suffices to determine its value.

The electromagnetic properties of the load material (sample to be heated) are simply input in the discretized versions of Eqs. 4 through 7, in the nodes corresponding to the space occupied by the load. No special boundary conditions need to be implemented at the interface between the empty part of the cavity and parts occupied by loads. Figure 5 shows the electric field strengths in the cavity with a TE_{11} source in the waveguide and a centered square load of one-third the linear dimension of the cavity. The load had the following electromagnetic properties; $\epsilon_{r,load} = 4$ F/m, $\mu_{r,load} = 1$ H/m and $\sigma_{load} = 0.01$ S/m. In Fig. 5, the qualitative features of the field are disturbed by the presence of the load, but since it is centered, the distortion is minimal. The magnitudes of the peak heights however, are significantly lowered. The inset shows the electric field over the load, the field strengths here are much smaller than the largest values developed in the empty part of the cavity.

The size and position of the loads also exert a significant influence on the electromagnetic fields. Samples smaller than a resonance cell, but still positioned in the center of the cavity serve to create a kind of radial symmetry surrounding the load. Loads positioned off-center create irregular patterns in the cavity. Examples are shown in Fig. 6.

6 Multimode simulation

Most microwave devices emit a range of frequencies, centered on the frequency which is given as a specification for the unit. Coupled with the cavity dimensions, this frequency range produces a number of simultaneous modes which can be summed up to produce an overall multimode character for the unit. In this present two dimensional study, only TE modes are considered, but for real cases, both TE and TM modes need to be calculated and summed.

Figure 7 shows a schematic of the frequency spectrum. A value known as a quality factor Q , is defined as,

$$Q = \frac{f_0}{\Delta f} \quad (13)$$

Setting a value for Q thus defines the range of frequencies and hence which indices m , n and l satisfy Eq. 12. Further, if the frequency distribution is assumed to be gaussian, the source amplitude of off-center frequencies can be calculated according to,

$$\frac{E_{mnl}}{E_0} = \exp\left(\frac{-2 \ln 2 Q^2 (f_{mnl} - f_0)^2}{f_0^2}\right) \quad (14)$$

6.1 Virtual waveguides

In cases where lateral symmetry is not obtained with the grid, a virtual waveguide is employed to achieve the required resonance in the cavity. This is the case when the mode index m is even.

In this case, a double sized or full-cavity width virtual waveguide is employed, thereby imparting symmetry

from the source to attain the desired resonance. This was seen to affect the amplitude of the peaks, and it can be corrected by noting the relation shown by Vegh et al. [19],

$$E_0 \propto \sqrt{\frac{P_0}{a}} \tag{15}$$

where P_0 is the average power output of the microwave generator. To verify the effect of double waveguides, tests were conducted with the TE₃₃ mode where the peak amplitudes could be compared with known results [17]. With two or three waveguides positioned across the face of the cavity, the functionality of Eq. 15 was respected. That is, if a virtual double wave guide is used

Fig. 9 The TE E and H fields for the multimode field produced from a 700 W source on a load of La₂NiO₄. The inset shows a higher resolution E field on the load specimen

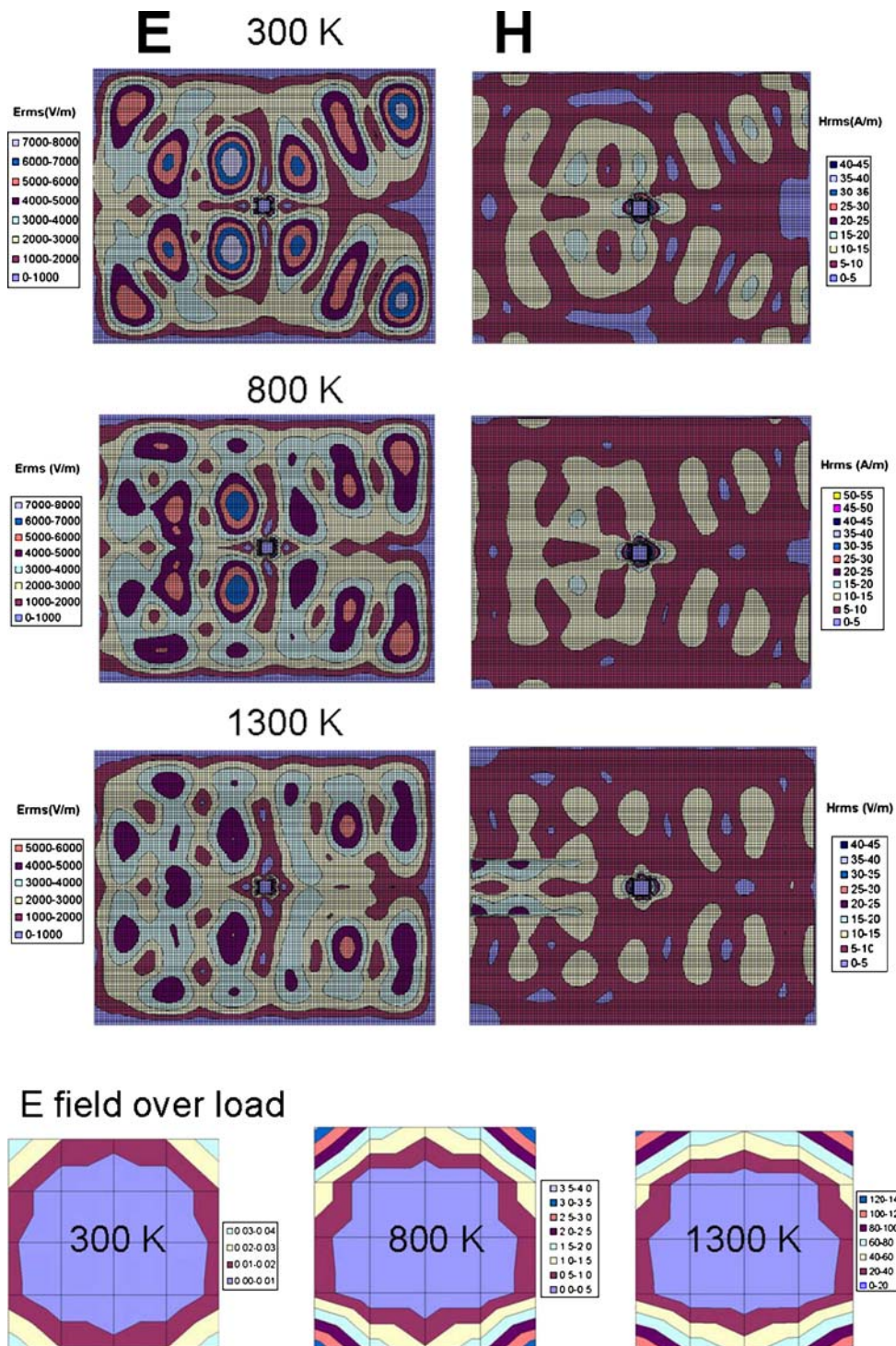


Table 1 Resonant TE modes in a 31.4 cm by 39.0 cm cavity, emitting at 2.45 GHz with a Q factor of 100.

Modes	m	n	f (GHz)	Amplitude coefficient
1	2	6	2.4976	0.005
2	3	5	2.3983	0.002
3	4	4	2.4532	0.977
4	5	1	2.4193	0.113
5	5	2	2.5093	0.0004

to achieve symmetry, the source amplitudes must be corrected by the factor of $\frac{1}{\sqrt{2}}$.

7 Multimode test case

7.1 Empty cavity

A trial was made to examine the multimode character of the empty cavity corresponding to the dimensions of our laboratory unit. Solution of Eq. 12 with $Q = 100$ gave the following set of modes detailed in Table 1.

The TE₄₄ mode dominates the multimode behaviour in this case since its frequency is near the specified frequency of 2.45 GHz, so its attenuation is minimal. The other four modes make only a minor difference to the resulting field. Figure 8 shows the five TE fields corresponding to the five modes determined and listed in Table 1.

7.2 SOFC material

An example simulation is described below. In connection with our aim of testing and developing novel SOFC materials, the electromagnetic fields developed around a sample made of lanthanum nickelate (La₂NiO₄) in a microwave cavity of dimensions matching an experimental unit in our laboratories were simulated.

For La₂NiO₄, the required material properties over a broad temperature range were assembled as described in [6]. A cavity of dimensions 31.4 by 39.0 cm was used. A square sample of edge length 1.884 cm was placed in the center of the cavity. A Q factor of 20 was chosen, and 12 modes were thus propagated in the cavity. Three temperatures were simulated, 300, 800 and 1300 K. Material parameters for these conditions are listed in Table 2.

Figure 9 shows the E and H fields for the three temperatures 300, 800 and 1300 K. Also shown are higher resolution insets of the E fields over the La₂NiO₄ samples. The temperature dependence of the dielectric properties show that the field values intensify in an exponential manner between 800K and 1300 K.

Reference [6] shows that the H field and the elevated magnetic loss properties of La₂NiO₄ produce the majority contribution to the heating rate, as per Eq. 1. P_{MW} contributions to the heat transport equation, Eq. 2, are given in Table 2 from both the E and H fields. Clearly, for the case of La₂NiO₄, the magnetic response to the microwave field is the main source of heat uptake. The result of a microwave heating measurement, and modeling the heat uptake considering the different combinations of E and H field contributions are shown in Fig. 10. The method of Torres and Jecko [20] was employed for implementing the heat transfer in the FDTD method.

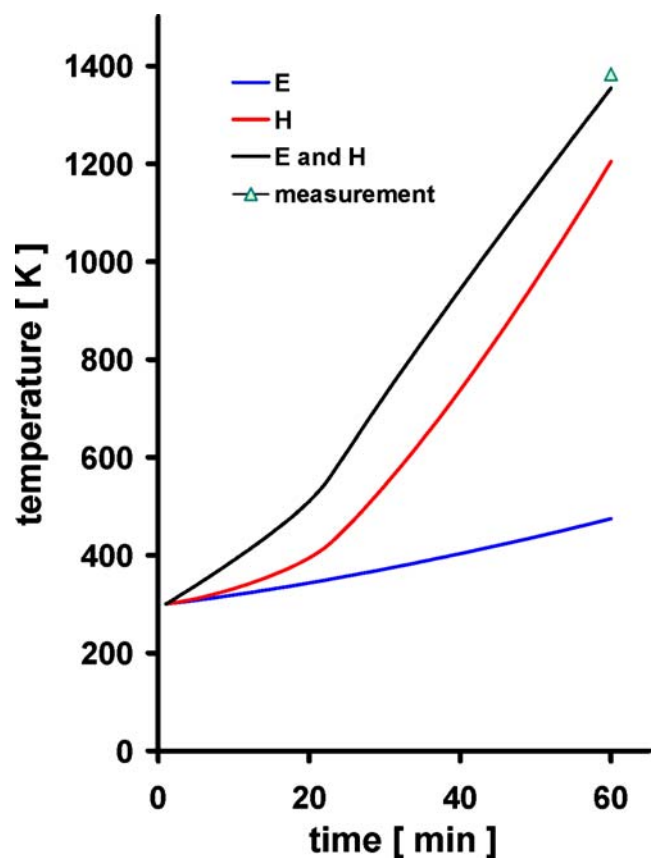


Fig. 10 Simulated temporal heating profiles for a 13 mm diameter disc of 2 mm thickness of La₂NiO₄, at 2.45 GHz and 300 W power. The different curves show simulation results where the E , H or both E and H field contributions to heating were activated. One experimental datum is also shown for comparison purposes

Table 2 Temperature dependent material properties of La_2NiO_4 .

T (K)	$\epsilon_r, \text{La}_2\text{NiO}_4$ (F/m)	$\mu_r, \text{La}_2\text{NiO}_4$ (H/m)	E (V/m)	H (T)	$P_{MW}(E)$ (J/[m ³ · s])	$P_{MW}(H)$ (J/[m ³ · s])
300	12.74	7.744×10^5	0.025	6.00×10^{-5}	2.64×10^{-18}	7.85×10^{-8}
800	14.93	8.535×10^3	3.04	6.04×10^{-3}	1.79×10^{-10}	3.39×10^{-7}
1300	15.99	1.699×10^2	101.2	0.77	1.36×10^{-13}	6.44×10^{-5}

|E| and |H| values are averaged over the load area.

8 Simulation in three dimensions

For good accuracy it will be necessary to extend the preceding formulations to three dimensions. At this point, TE and TM mode calculations have been carried out at the code validation stage on empty cavities. In these cases, all six components of the combined E and H fields must be evaluated. Figure 11 shows the composite E field for a 333 mode with contributions from both the TE and TM fields. The largest E field values here are seen to be around 5.0×10^4 V/m, compared to values around 3.0×10^4 V/m for the two dimensional case shown in Fig. 2. In this three dimensional case the peak TE E field values were around 2.8×10^4 V/m, close to the values obtained with the two dimensional simulation. The additional field strength in the three dimensional case comes from the TM mode contributions, which were not considered in the two dimensional work. The ability to incorporate spatial properties from fundamentally determined three dimensional electromagnetic fields into a transient microstructure based sintering simulation represents a novel advance in computational materials science.

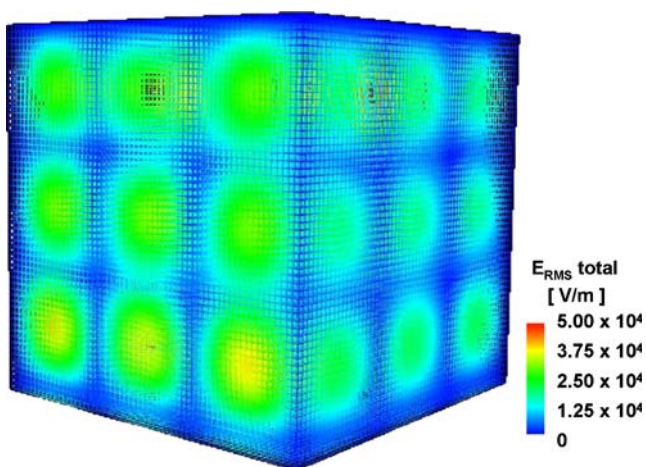


Fig. 11 The combined TE and TM contributions to the E field in a cavity resonating in 333 mode

9 Conclusions

This simulation is thus poised to serve as a very useful research tool for sintering operations connected to SOFC electrode development. Electromagnetic fields in good spatial resolution were able to be calculated in two dimensions over samples placed in microwave cavities. The project is currently being extended to three dimensional capability.

Novel advances of the present study include coupling the resonant mode determination scheme with the FDTD method to calculate multimode electromagnetic fields based on fundamental system parameters. The presentation and analysis of the different temporal behaviour for loaded and unloaded cavities demonstrates explicitly FDTD methodology previously unreported. The implementation of virtual waveguides for modes of even values of the index m , is an original contribution to the FDTD method. Finally, demonstrating use of both the E and H fields as relevant components of microwave heating is a novel application and validation of the FDTD method.

Since the sintering simulation for which the present electromagnetic component was developed, handles the particle size distribution as a local field variable, microstructure control can be achieved by fine tuning power inputs as well as judiciously preparing powders with distribution qualities amenable to good sintered properties. Further uses are envisioned for defining processing tolerances in powder compact properties to avoid defects, cracks and/or thermal runaway.

References

1. D. Dadon, D.L. Martin, M. Rosen, A. Birman, D. Gershon, J.P. Calame, B. Levush, Y. Carmel, J. Mater. Synth. Process. **4**(2), 95–103 (1996)
2. K.H. Brosnan, G.L. Messing, D.K. Agrawal, J. Am. Cer. Soc. **86**(8), 1307–1312 (2003)
3. A. Rabenau, P. Eckerlin, Acta Cryst. **11**, 304–306 (1958)
4. A. Birnboim, Y. Carmel, J. Am. Ceram. Soc. **82**(11), 3024–3030 (1999)
5. R. Roy, R. Peelamedu, C. Grimes, J. Cheng, D. Agrawal, J. Mater. Res. **17**(12), 3008–3011 (2002)
6. K. Darcovich, P.S. Whitfield, G. Amow, K. Shinagawa, R.Y. Miyahara, J. Eur. Ceram. Soc. **25**(12), 2235–2240 (2005)

7. A. Birman, B. Levush, Y. Carmel, D. Gershon, D. Dadon, L.P. Martin, *Ceram. Trans.* **59**, 305–12 (1995)
8. K.S. Yee, *IEEE Trans. Antennas Propag.* **AP-14**(3), 302–307 (1966)
9. P.C. Cherry, M.F. Iskander, *Microwave Theory Tech.* **40**(8), 1692–1700 (1992)
10. M.F. Iskander, R.L. Smith, A.O.M. Andrade, H. Kimrey Jr., L.M. Walsh, *IEEE Trans. Microwave Theor. Tech.* **42**(5), 793–800 (1994)
11. M.J. White, M.F. Iskander, Z. Huang, *IEEE Trans. Antennas Propag.* **45**(10), 1512–1517 (1997)
12. D.D. Dinkov, K.A. Parrot, *Computational analysis of microwave heating patterns in resonant multimode cavities*. Proc. 2004 ACM Symp. Applied Computing, (Nicosia, Cyprus, Mar. 14-17, 2004), pp. 215–219
13. J. Tucker, M.F. Iskander, Z. Huang, *Mat. Res. Soc. Symp. Proc.* **347**, 353–362 (1994)
14. M.J. White, M.F. Iskander, H.D. Kimrey, *Mat. Res. Soc. Symp. Proc.* **420**, 325-331 (1996)
15. A.J. Baden Fuller, *Microwaves, An Introduction to Microwave Theory and Techniques*, 3rd edn. (Pergamon Press, Oxford, 1990)
16. A. Taflove, S.C. Hagness, *Computational Electrodynamics, the Finite-difference Time-domain Method*, 2nd edn. (Artech House, Boston, 2000)
17. J. Clemens, C. Saltiel, *Int J. Heat Mass Transfer.* **39**, 1665–1675 (1996)
18. S. Ramo, J.R. Whinnery, T. Van Duzer, *Fields and Waves in Communication Electronics*, 3rd edn. (Wiley, New York, 1994)
19. V. Vegh, I.W. Turner, E. Sizgek, D. Sizgek, *ANZIAM J.* **45**(E), C34-C49 (2004)
20. F. Torres, B. Jecko, *IEEE Trans. Microwave Theor. Tech.*, **45**(1), 108–117 (1997)